Multiple growth of graphene from a pre-dissolved carbon source

PAPER • **OPEN ACCESS**

Multiple growth of graphene from a pre-dissolved carbon source

To cite this article: Andrea Fazi *et al* 2020 *Nanotechnology* **31** 345601

OPEN ACCESS
IOP Publishing
Nanotechnology

Nanotechnology **31** (2020) 345601 (10pp)
https://doi.org/10.1088/1361-6528/ab9040

Multiple growth of graphene from a pre-dissolved carbon source

Andrea Fazi[1,2,6], Andreas Nylander[1,6], Abdelhafid Zehri[1], Jie Sun[2,3], Per Malmberg[4], Lilei Ye[5], Johan Liu[1] and Yifeng Fu[1]

[1] Electronics Materials and Systems Laboratory, Department of Microtechnology and Nanoscience, Chalmers University of Technology, SE-412 96, Gothenburg, Sweden
[2] Quantum Device Physics Laboratory, Department of Microtechnology and Nanoscience, Chalmers University of Technology, SE-412 96, Gothenburg, Sweden
[3] Key Laboratory of Optoelectronics Technology, College of Microelectronics, Beijing University of Technology, Beijing 100124 People's Republic of China
[4] Department of Chemistry and Chemical Engineering, Chalmers University of Technology, Gothenburg, Sweden
[5] SHT Smart High Tech AB, Kemivägen 6, 412 58, Gothenburg, Sweden

E-mail: jie.sun@chalmers.se and yifeng.fu@chalmers.se

Received 15 December 2019, revised 8 April 2020
Accepted for publication 5 May 2020
Published 9 June 2020

Abstract

Mono- to few-layer graphene materials are successfully synthesized multiple times using Cu-Ni alloy as a catalyst after a single-chemical vapor deposition (CVD) process. The multiple synthesis is realized by extracting carbon source pre-dissolved in the catalyst substrate. Firstly, graphene is grown by the CVD method on Cu-Ni catalyst substrates. Secondly, the same Cu-Nicatalyst foils are annealed, in absence of any external carbon precursor, to grow graphene using the carbon atoms pre-dissolved in the catalyst during the CVD process. This annealing process is repeated to synthesize graphene successfully until carbon is exhausted in the Cu-Ni foils. After the CVD growth and each annealing growth process, the as-grown graphene is removed using a bubbling transfer method. A wide range of characterizations are performed to examine the quality of the obtained graphene material and to monitor the carbon concentration in the catalyst substrates. Results show that graphene from each annealing growth process possesses a similar quality, which confirmed the good reproducibility of the method. This technique brings great freedom to graphene growth and applications, and it could be also used for other 2D material synthesis.

Supplementary material for this article is available online

Keywords: graphene, multiple growth, alloy

(Some figures may appear in colour only in the online journal)

1. Introduction

Graphene is a single layer of carbon atoms organized in a honeycomb structure (sp^2 hybridized) and it has been isolated and characterized for the first time by Novoselov *et al* in 2004 [1]. Rapidly, it attracted the interest of the entire scientific community and became one of the most investigated materials in the past decade [2–4] due to its special structure and outstanding electrical [1, 3, 5, 6], thermal [7] and mechanical properties [8, 9]. Many applications based on graphene have been proposed and demonstrated in electronics, including graphene-based transistors [10], transparent electrodes [11], heat spreaders [12–16], touchscreens [17], light-emitting diodes [18, 19], solar cells [20] and foldable electronics [21]. Beyond that, thanks to its special features, graphene can be also applied in biomedicine and

[6] These authors contributed equally to the paper

biology [22, 23]. A few methods have been developed to synthesize graphene material, including tape-assisted mechanical cleavage [1], SiC-based sublimation [24–26], chemical vapor deposition (CVD) [27, 28], and liquid phase exfoliation [4, 29]. Among them, the CVD method allows controllable growth of transferrable mono-layer graphene with high quality and good repeatability [30]. In the CVD process, transition metals such as Cu, Ni, Pt, etc [31, 32] are often used as a catalyst to grow graphene. Cu allows controllable growth of 1–2 layers of graphene [28, 33], while Ni [34] and Pt [35] commonly catalyze graphene growth with multiple layers since the solubility of carbon in Ni and Pt is much higher than that in Cu [36, 37]. Recently, metal alloys are also applied as catalysts to grow single crystalline graphene at high speed and to grow graphene with controllable thickness [38, 39]. In this paper, Cu-Ni alloy is selected as a catalytic substrate for graphene synthesis. The adopted alloy combines the ability of Cu to grow large area mono- to bi-layer graphene [33, 40], with the capability of Ni to store carbon atoms inside the alloy substrate [41]. With the use of this technique, pre-saturated alloys can be stored and used later without the need for CVD fabrication equipment and precursor gases. This method would also provide a fabrication route for graphene-based devices which would circumvent the issue with graphene degradation when subjected to different fabrication processes like etching or solvent processing. By using this method, mono- to few-layer graphene materials (1–3 layers) are successfully synthesized multiple times from a single CVD process. To the best of our knowledge, the concept of multiple graphene synthesis demonstrated in this paper is the first of the kind.

2. Experimental methods

The experimental process is illustrated in figure 1. First, 50 μm thick Cu-Ni alloy foils (GoodFellow, Cu55/Ni45) are prepared in the size of 3 $\times$ 4 cm^2 (figures 1(a) and S1 (avaliable online at stacks.iop.org/Nano/31/345601/mmedia) in supplementary material). Before graphene growth, the alloy foils are cleaned in acetic acid for 5 min to remove the native oxides on the surface and followed by 5 min cleaning in acetone and deionized water respectively. Second, each Cu-Ni substrate is subjected to a thermal CVD process using acetylene (C_2H_2) as a carbon precursor to grow graphene on the foil surface. In the meantime, extra carbon atoms are dissolved inside the Cu-Ni alloy (figure 1(b)). Afterwards, the obtained graphene is transferred onto Si/SiO_2- substrates using the bubbling transfer method [42] for further characterizations, as shown in figures 1(c) and S2. Then the Cu-Ni substrate is annealed under the same temperature in the same CVD chamber but without supplying any external carbon source. During the annealing, new graphene is grown on the surface of the Cu-Ni foil using the carbon source that is stored inside the alloy during the CVD process, as shown in figure 1(d). Once the first annealing is completed, the new-grown graphene film is transferred onto Si/SiO_2- substrates using the same bubbling method (figure 1(e)) and the Cu-Ni substrate is re-used for the second annealing to grow graphene (figure 1(f)). This sequence of operations are repeated five times until the carbon source in the Cu-Ni substrate are completely consumed, and graphene is successfully synthesized after each annealing process.

The growth of graphene thin films is performed in a cold wall CVD system (Aixtron, Black Magic 2-inch) on Cu-Ni alloy substrates (Cu55 wt.%–Ni45 wt.%). The CVD growth process is performed using 40 sccm C_2H_2 as a carbon precursor and 1000 sccm argon (Ar) as carrying gas. Before the graphene growth starts, the Cu-Ni foil is reduced at 850 °C for 5 min in 25 sccm H_2 environment. While the annealing growth process uses only 1000 sccm Ar as the carrying gas and 25 sccm H_2 reducing gas but without any C_2H_2. The substrate temperature and the process pressure in the chamber (for both the CVD growth and the followed annealing growth) are fixed at 850 °C and ~6 mbar, respectively. 0.3 mol l^{-1} NaOH aqueous solution electrolyte is used for the bubbling transfer of graphene. With a current of 0.2 A, the PMMA supported graphene is completely separated from the growth substrate after about 5 min. Si substrates, on which a 300 nm thick SiO_2 was previously deposited, are chosen as the target transfer substrates for easy optical observation of the graphene materials. Both the CVD growth and annealing growth processes are performed for 10 min in the same CVD system.

The as-transferred graphene materials are then characterized with different methods and equipments. Optical microscopy (Olympus MX50) is applied to observe the coverage and uniformity of the graphene on the Si/SiO_2 substrate. With the assistance from ImageJ (image processing software), the distribution of graphene layers is analysed statistically. Raman spectroscopy and Raman mapping are conducted by Horiba XploRA to examine the overall quality of the graphene. Transmission electron microscopy (TEM) is applied to observe the crystallinity and defects in the graphene films. Sheet resistance of the transferred graphene is measured with an AIT CMT-SR2000 N 4-point probe system. The concentration of carbon in the Cu-Ni foils is measured through secondary ions mass spectroscopy (SIMS) both after the CVD growth and after each annealing growth.

3. Results and discussion

The difference in the number of layers causes graphene film to display different colours on certain substrates due to the light interference effect [43, 44]: shifting through pink, purple, blue and white from single-layer graphene to thin graphite sheet (for instance in figure S3 in the supplementary material). Optical images of the graphene films grown on the Cu-Ni foils and then transferred onto the Si/SiO_2 substrates are presented in figure 2. Figure 2(a) shows the graphene film grown from the CVD process. It can be seen that the film contains many thin graphite islands (the purple and white areas) since there is redundant carbon source during the CVD growth. Figure 2(b) shows the optical image of the graphene film grown from the 1st annealing process. Some graphite islands are still visible in this film but most of the area is covered by 1–3 layers

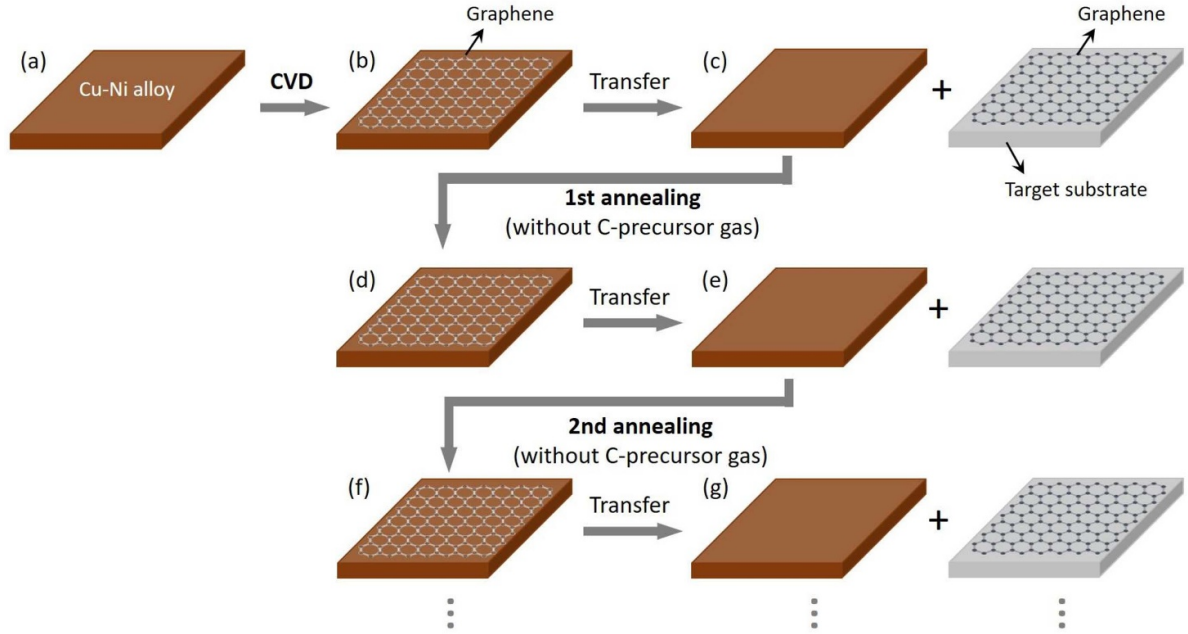

Figure 1. Sketch of the experimental procedure: (a) Cleaned Cu-Ni alloy foil. (b) CVD growth of graphene on the Cu-Ni alloy substrate. (c) Graphene film transfer by the bubbling method. (d) The 1st annealing growth of graphene on the Cu-Ni substrate without an external carbon source. (e) Graphene film transfer by the bubbling method. (f) The 2nd annealing growth of graphene on the Cu-Ni substrate without external carbon source. (g) Graphene film transfer by the bubbling method and the whole process is repeated until the carbon source is exhausted in the Cu-Ni substrate.

of graphene. The number of graphene layers is identified by optical observation and supported by TEM images and Raman spectra. First, a crack generated during transfer is found on the graphene material (as shown in figure S3) and it is used as the reference (the exposed SiO_2 surface). Second, a transition area with different thickness of graphene is found so that the number of graphene layers can be directly counted (figure S3). The optical observation is further supported by TEM and Raman spectra in figures 4 and 5, which allow precise measurements of graphene thickness in a local area.

Figures 2(c)–(e) show graphene materials grown from the 2nd annealing to the 4th annealing. It can be seen that the graphene materials are very uniform with little thin graphite islands and holes. In contrast, the 5th annealing process produced a graphene film made of monolayer graphene with more blank area that is not covered by graphene. This is because the carbon source dissolved in the catalyst substrate is completely consumed so there is not sufficient carbon atoms to grow a full graphene layer. This is further confirmed by the measurement of carbon concentration in the catalyst substrate as shown in figure 8. Optical images from figures 2(b)–(e) clearly show that the graphene films grown from the annealing processes are similar to each other in terms of thickness and uniformity. The graphene materials grown from the CVD and various annealing processes are categorized by thin graphite islands, 1–3 layers of graphene and blank Si areas. The coverage percentage of the graphene materials is calculated by the ImageJ software and the result is shown in figure 3. More details about the statistics analysis are explained in figure S4 in the supplementary material. From figure 3, it can be seen that most of the 'graphene' material grown from the CVD process is actually thin graphite islands, and the 1st annealing to the 4th annealing processes produced mostly 1–3 layers of graphene. From the 3rd annealing process, blank areas (without graphene) started to appear and it increased significantly (∼30%) in the graphene grown from the 5th annealing process. These are in accordance with the optical observation in figure 2. It should be also pointed out that the issue associated with the uncovered area, however, is not only intrinsic, as the transfer process also brings damages on the graphene film [45, 46].

Figures 4(a)–(f) show the TEM images of the thin graphite islands grown from the CVD process and the graphene grown from the annealing processes, respectively. It can be seen that very thick graphene films (thin graphite islands) are commonly observed in figure 4(a) while 1–3 layers of graphene is found in figures 4(b)–(f), which is consistent with the results in figures 2 and 3. The inset in figure 4(f) shows the electron diffraction pattern of the graphene grown from the 5th annealing.

The graphene materials are further characterized by Raman spectroscopy after being transferred onto the Si/SiO_2 substrate. Figure 5 shows the Raman spectra of graphene materials grown from each step. In each spectrum, the characteristic D, G and 2D peaks for graphene can be found at around 1350 cm^{-1}, 1600 cm^{-1} and 2750 cm^{-1}, respectively. In figure 5(a), the D peak is very low, indicating low density of defects in the graphene crystals grown from the CVD process, whereas the low 2D/G ratio indicates the thickness of the graphene film is very high, which is consistent with the results in figures 2–4. The Raman spectra in figures 5(b)–(e) are similar to each other, all of them have a relatively high 2D/G ratio, indicating mono-layer graphene in the inspected

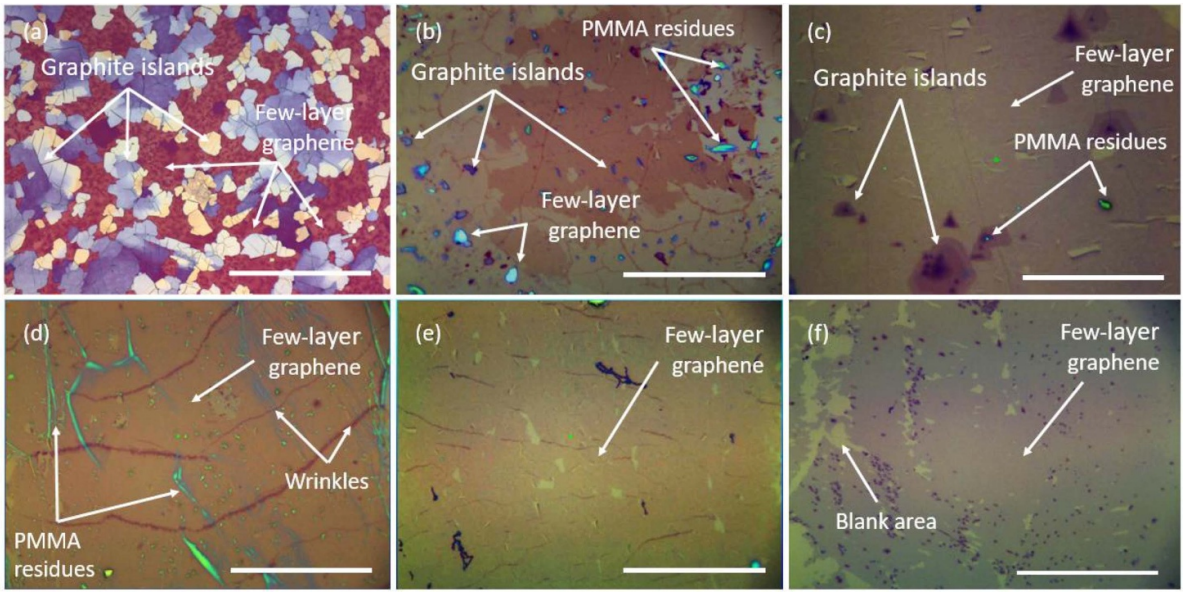

Figure 2. Optical microscopy images of the transferred graphene grown from the CVD process (a), from the 1st annealing (b), from the 2nd annealing (c), from the 3rd annealing (d), from the 4th annealing (e) and from the 5th annealing process (f). (Scale bars 100 μm).

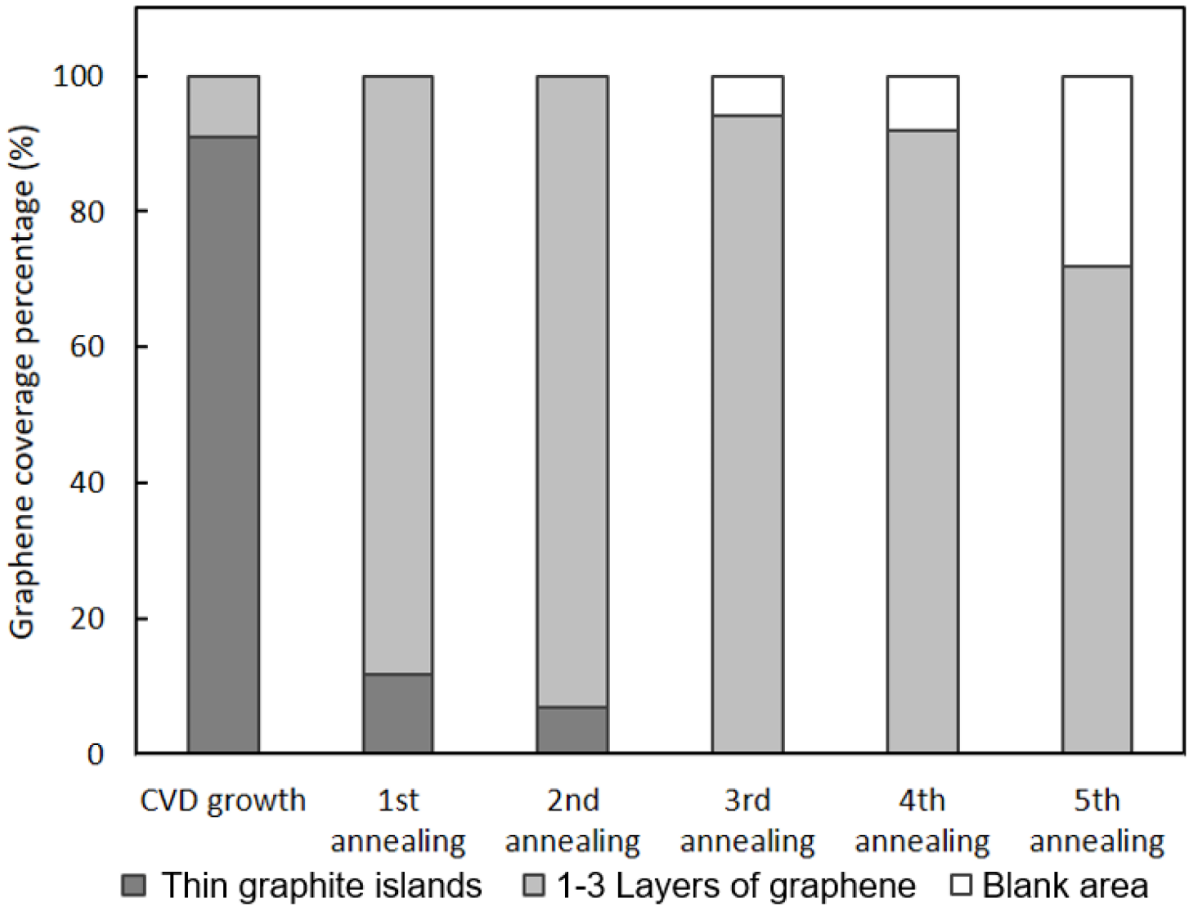

Figure 3. Coverage percentage of graphene after the CVD and annealing growth processes.

area. However, the D peaks in figures 5(b)–(e) are much higher than that of in figure 5(a), which means the graphene materials grown from the annealing processes have more defects than that grown from the CVD process. The Raman spectrum in figure 5(f) has a very high D peak and relatively low G and 2D peaks, which indicates high density of defects in the graphene

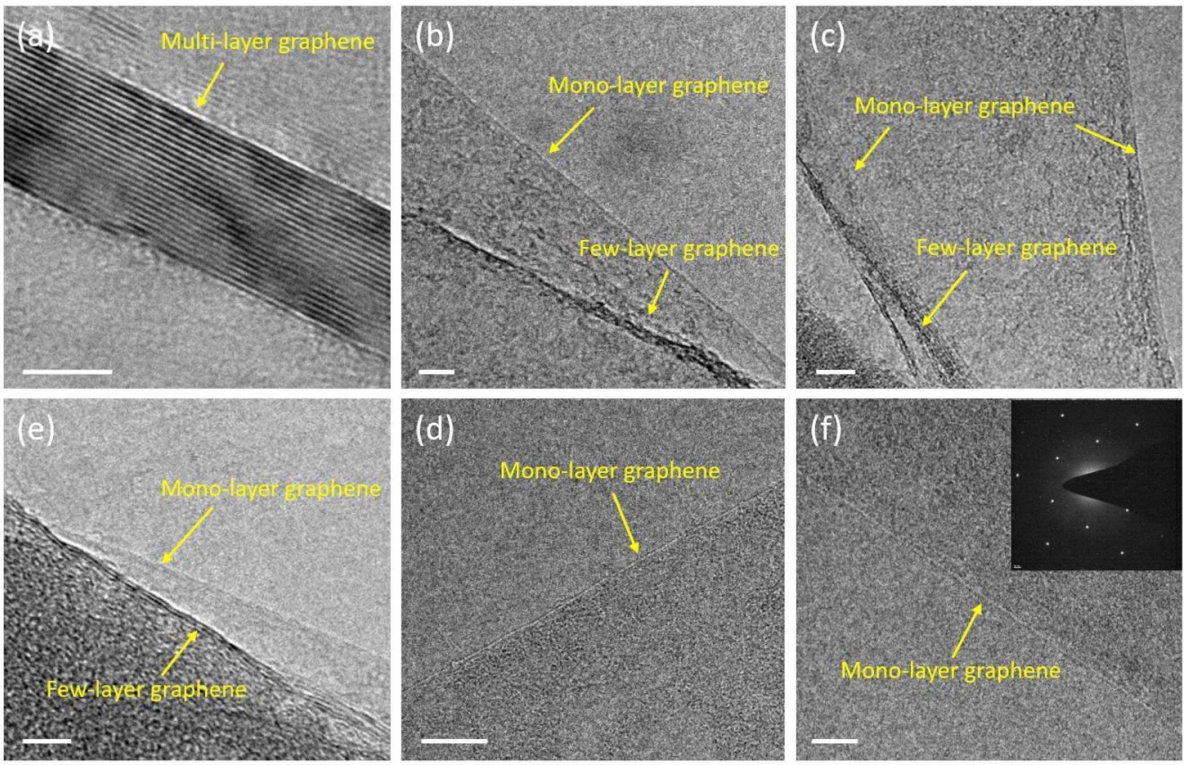

Figure 4. (a) TEM image of multi-layer graphene grown from the CVD process. (b)–(e) Mono-to few-layer graphene grown from the 1st, 2nd and 3rd annealing processes. (d)–(f) Mono-layer graphene grown from the 4th and 5th annealing processes. Scale bar: 5 nm. Inset in (f): electron diffraction pattern of the monolayer graphene.

crystals because carbon atoms have been exhausted in the catalyst substrate so there is not enough carbon source to sustain the growth of a full graphene layer. Additionally, a split G peak can be observed in figure 5(f), which further confirms the high density of defects in the graphene material and is consistent with previous Raman studies on high-defect mono-layer graphene [47]. It should also be noticed that the Raman spectra in figure 5 can only show the quality of graphene in a small region, the overall quality of the graphene materials is further examined by Raman mapping.

As shown in figure 6, Raman mapping is performed for the graphene materials after being transferred onto the Si/SiO_2 substrates. Figures 6(a) and (b) show the D/G ratio and 2D/G ratio respectively for the graphene grown from the CVD process. The low D/G ratio (figure 6(a)) and low 2D/G ratio (figure 6(b)) confirm that the white-purple patches in figure 2(a) are indeed high quality multi-layer graphene sheets (or thin graphite islands) [48]. Figures 6(c)–(f) and (h)–(l) are Raman mapping for the graphene grown from the 1st, 2nd, 3rd, 4th and 5^{th} annealing process, respectively. It can be seen that the D/G ratio in these materials becomes higher and higher, which means more and more defects appear in the graphene material after each annealing growth. It can be also seen that the 2D/G ratio continuously increases from figures 6(b) to (j), which implies that the layer number of graphene material decreases continuously. However, in figures 6(k)–(l), the D/G ratio increases and 2D/G ratio decreases significantly since the carbon source is exhausted in the catalyst substrates. This also agrees well with the results in figures 2, 3 as well as in figure 5.

After being transferred onto the Si/SiO_2 substrates, sheet resistances of the graphene films are measured and presented in figure 7. It can be seen that the sheet resistance of the graphene with many thin graphite islands grown from the CVD process is around 0.6 kΩ/square, while the graphene films grown from the 1st to the 3rd annealing processes have a very stable but much higher sheet resistance of around 25 kΩ/square. This means that the graphene films grown from the 1st to the 3rd annealing are quite reproducible but much thinner than that grown from the CVD process. Afterwards, the sheet resistance of the graphene film grown from the 4th annealing starts to increase and reaches 53 kΩ/square at the 5th annealing growth. These results further confirm the observation and measurements in figures 2 and 3.

In order to verify the growth mechanism and understand the growth process, we used SIMS to monitor the concentration of carbon in the catalyst substrate. Figure 8 shows the change of the concentration of carbon in the Cu-Ni foils throughout the CVD and annealing growth processes. More details about the SIMS analysis is explained in the supplementary material. As shown in figure 8, after the CVD growth, the concentration of carbon in the Cu-Ni catalyst substrate is around 0.58 at%, which is the amount of carbon atoms dissolved in the Cu-Ni alloy. Afterwards, the concentration of carbon continuously decreases because the carbon atoms are consumed for graphene growth after each annealing process. After the 4th

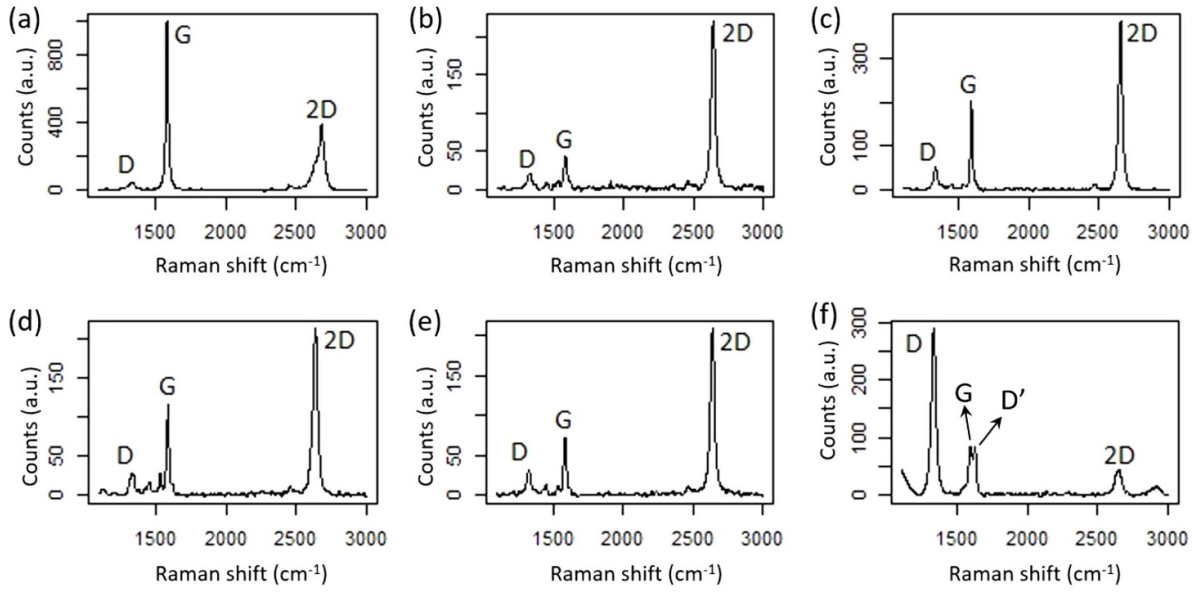

Figure 5. Raman spectra of the graphene films transferred onto Si/SiO_2 substrates. (a) Graphene grown from the CVD process. (b) Graphene grown from the 1st annealing process. (c) Graphene grown from the 2nd annealing process. (d) Graphene grown from the 3rd annealing process. (e) Graphene grown from the 4th annealing process. (f) Graphene grown from the 5th annealing process.

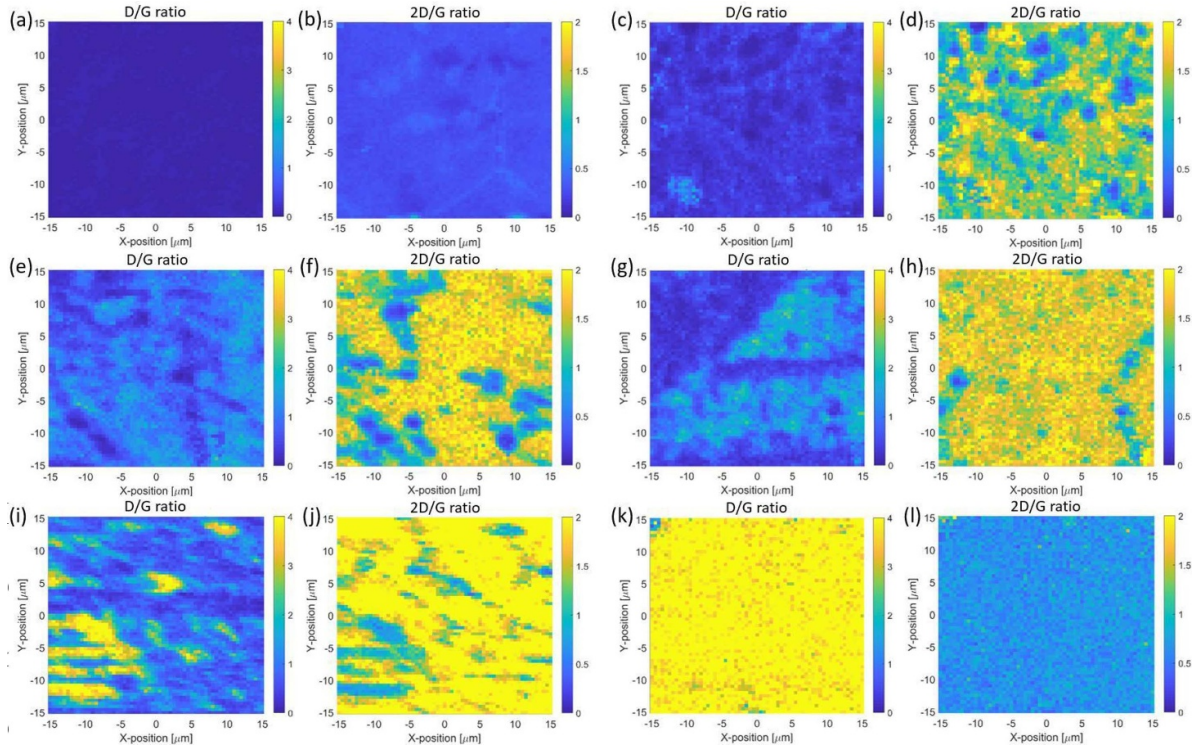

Figure 6. Raman mapping of the transferred graphene films on Si/SiO_2 substrates. D/G ratio (a) and 2D/G ratio (b) of the graphene grown from the CVD process. D/G ratio (c) and 2D/G ratio (d) of the graphene grown from the 1st annealing process. D/G ratio (e) and 2D/G ratio (f) of the graphene grown from the 2nd annealing process. D/G ratio (g) and 2D/G ratio (h) of the graphene grown from the 3rd annealing process. D/G ratio (i) and 2D/G ratio (j) of the graphene grown from the 4th annealing process. D/G ratio (k) and 2D/G ratio (l) of the graphene grown from the 5th annealing process.

annealing growth, the concentration of carbon is almost stabilized which results in an incomplete graphene growth during the 5th annealing process, which is also supported by figure 2(f). This also means that the minimum concentration of carbon in Cu-Ni alloy is around 0.412 at.% to enable high quality graphene growth.

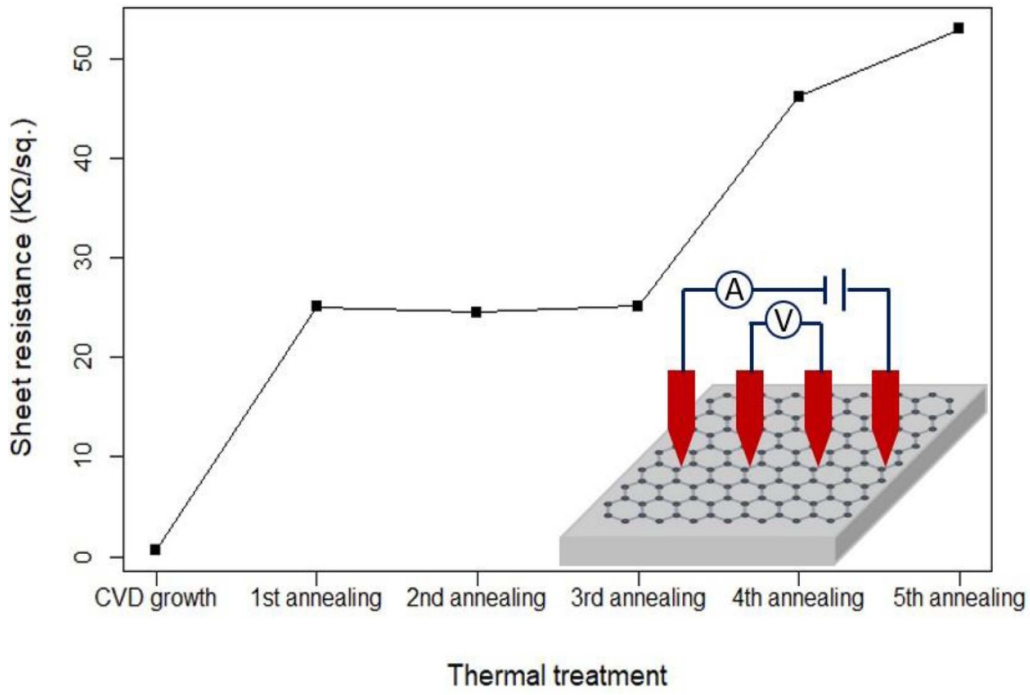

Figure 7. Sheet resistance of the transferred graphene from the CVD and annealing growth processes. Inset: 4-probe measurement of graphene sheet resistance.

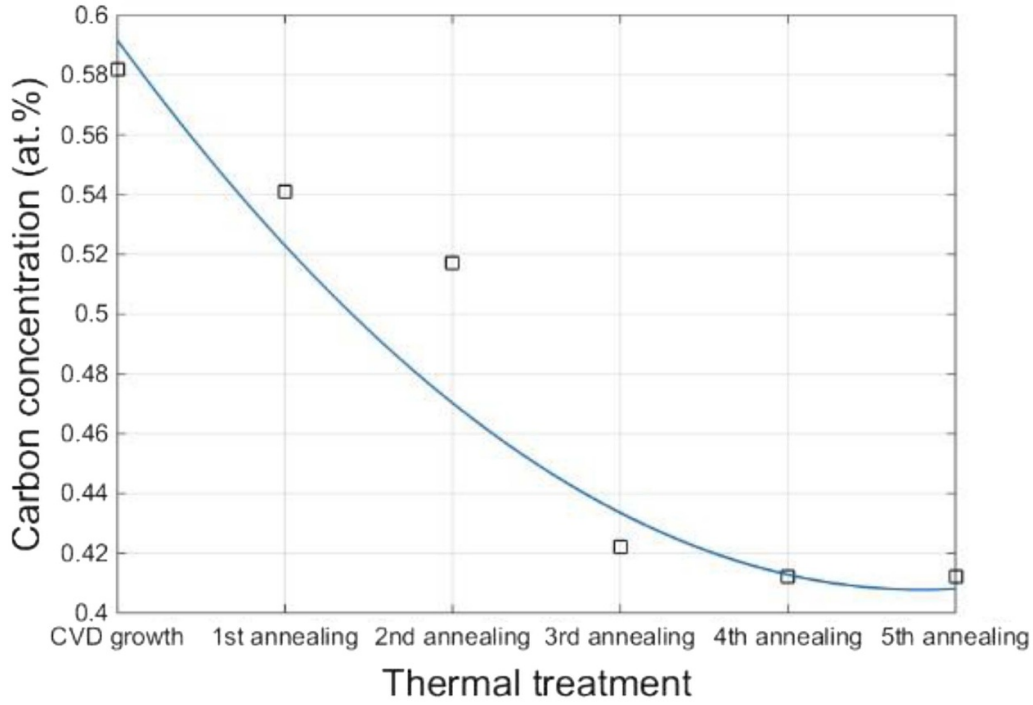

Figure 8. SIMS analysis on the concentration of carbon in the Cu-Ni metal alloy after the CVD and each annealing growth process.

From the results presented above, the mechanism for the graphene growth from the Cu-Ni alloy can be understood (as illustrated in figure 9). During the CVD growth process, the carbon precursor gas (acetylene in this work) decomposes on the surface of the Cu-Ni foil [49–51] which acts both as a substrate and as a catalyst for the graphene growth. At high temperature, the carbon atoms will react to form graphene layers or thin graphite islands. Meanwhile, some carbon atoms will diffuse into the Cu-Ni alloy and be stored in the lattice as interstitial atoms to form a solid solution [36, 37, 41]. The graphene grown on the surface of the alloy is then transferred and characterized. When the alloy is annealed at 850 °C, the

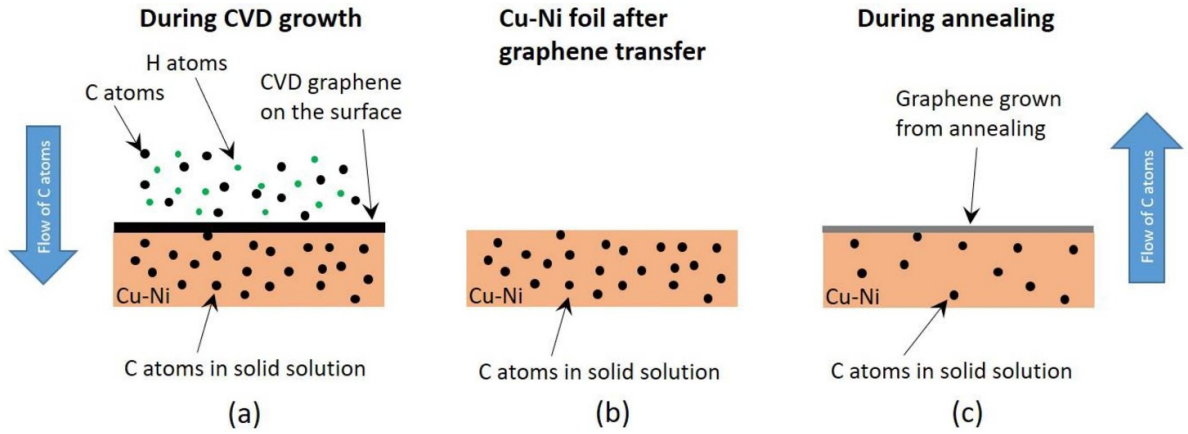

Figure 9. A schematic of the process dynamics is presented. (a) During the CVD the precursor carbon-containing gas decomposes into carbon atoms on the surface of the Cu-Ni metal foil. Some of the carbon atoms form graphene on the surface, some others diffuse into the metal foil. (b) Once the graphene is removed from the surface of the Cu-Ni metal foil, the only carbon remaining is in the forms of atoms inside the crystal lattice. (c) During the annealing the high temperature increases the diffusion rate of the carbon atoms trapped in the crystal lattice and set them free to migrate towards the surface to form a new layer of graphene.

high temperature enables some of the carbon atoms to diffuse towards the surface of the foil to act as the carbon source in the formation of the new graphene film. Nevertheless, after the 5th annealing, it is evident that the carbon source in the Cu-Ni alloy has been exhausted, i.e. the concentration of carbon in the catalyst substrate is too low to enable the growth of a complete graphene mono-layer.

In addition, we can roughly estimate the solubility of carbon in the Cu-Ni alloy. The solubilities of carbon in Cu and Ni are about 0.00045 at.% [52] and 0.9 at.% [53] at around 850 °C, respectively. Therefore, the nominal carbon concentration in the 55%-Cu 45%-Ni alloy is around $(0.00045 \times 0.55 + 0.9 \times 0.45)$ at.% $= 0.405$ at.%. According to the SIMS analysis in figure 8, the concentration of carbon in the catalyst alloy after the CVD growth was about 0.58 at%, which is slightly higher than the theoretical solubility of carbon in the Cu55Ni45 alloy, meaning carbon was actually supersaturated after the CVD growth and being gradually consumed during the annealing growth processes. It should also be noticed that the final concentration of carbon in the Cu-Ni alloy is around 0.412 at.% which is very close to value. This is also consistent with the dissolve-segregation-based growth mechanism.

4. Conclusions

This work proved that it is possible to realize multiple graphene growth from a single CVD process by repeatedly annealing the catalyst substrate. This concept is new and to the best of our knowledge it has not reported before. The method demonstrated in this paper brings great freedom to graphene synthesis and various applications. For example, the method could be very useful for long-term reliable storage of graphene. From the fundamental research point of view, the study provides insights on graphene growth dynamics that helps us to understand the role of metal catalysts in this process. This new method could be further optimized by using different compositions of the alloy to realize more precise control on the graphene layers and a higher number of annealing steps before depletion of the carbon source. In addition, the concept presented in this paper could be applied to other metal alloys and to other 2D material synthesis.

Acknowledgments

A Nylander, J Liu and Y Fu acknowledge the financial support from the Swedish National Science Foundation with the contract No: 621-2007-4660, from the Swedish Board for Innovation (Vinnova) within the Siografen Program, from the Swedish Board for Strategic Research (SSF) with the contract No: SE13-0061, from Formas with the contract No: FR-2017/0009, from EU project Nanosmart (825430), from the Production Area of Advance at Chalmers University of Technology, Sweden. In addition, Y Fu acknowledges the financial support from the Nano Area of Advance at Chalmers (Contract No: C 2017-1256). J Sun acknowledges the support from NFSC (11674016), NKRDPC (2017YFB0403102), BMCST (Z161100002116032), BMCE (PXM2017_014204_500034), and STINT (CH2015-6202).

ORCID iDs

Abdelhafid Zehri https://orcid.org/0000-0002-6129-0537
Johan Liu https://orcid.org/0000-0001-9931-1439
Yifeng Fu https://orcid.org/0000-0001-7783-8766

References

[1] Novoselov K S, Geim A K, Morozov S V, Jiang D, Zhang Y, Dubonos S V, Grigorieva I V and Firsov A A 2004 Electric field effect in atomically thin carbon films *Science* **306** 666–9
[2] Leenaerts O, Partoens B and Peeters F M 2008 Graphene: a perfect nanoballoon *Appl. Phys. Lett.* **93** 193107

[3] Geim A K and Novoselov K S 2007 The rise of graphene *Nat. Mater.* **6** 183–91
[4] Novoselov K S, Fal′ko V I, Colombo L, Gellert P R, Schwab M G and Kim K 2012 A roadmap for graphene *Nature* **490** 192–200
[5] Dugu S, Pavunny S P, Limbu T B, Weiner B R, Morell G and Katiyar R S 2018 A graphene integrated highly transparent resistive switching memory device *APL Mater.* **6** 058503
[6] Zhang Y, Tan Y-W, Stormer H L and Kim P 2005 Experimental observation of the quantum Hall effect and Berry's phase in graphene *Nature* **438** 201–4
[7] Balandin A A, Ghosh S, Bao W, Calizo I, Teweldebrhan D, Miao F and Lau C N 2008 Superior thermal conductivity of single-layer graphene *Nano Lett.* **8** 902–7
[8] Settembrini F F, Colangelo F, Pitanti A, Miseikis V, Coletti C, Menichetti G, Colle R, Grosso G, Tredicucci A and Roddaro S 2016 Anisotropic straining of graphene using micropatterned SiN membranes *APL Mater.* **4** 116107
[9] Frank I W, Tanenbaum D M, van der Zande A M and McEuen P L 2007 Mechanical properties of suspended graphene sheets *J. Vac. Sci.Technol.* B **25** 2558–61
[10] Schwierz F 2010 Graphene transistors *Nat. Nanotechnol.* **5** 487–96
[11] Wassei J K and Kaner R B 2010 Graphene, a promising transparent conductor *Mater. Today* **13** 52–59
[12] Yan Z, Liu G, Khan J M and Balandin A A 2012 Graphene quilts for thermal management of high-power GaN transistors *Nat. Commun.* **3** 827
[13] Subrina S, Kotchetkov D and Balandin A A 2009 Heat removal in silicon-on-insulator integrated circuits with graphene lateral heat spreaders *IEEE Electron Device Lett.* **30** 1281–3
[14] Gao Z, Zhang Y, Fu Y, Yuen M M F and Liu J 2013 Thermal chemical vapordeposition grown graphene heat spreader for thermal management of hot spots *Carbon* **61** 342–8
[15] Gao Z, Zhang Y, Fu Y, Yuen M and Liu J 2012 Graphene heat spreader for thermal management of hot spots in electronic packaging *18th Int. Workshop on THERMal INvestigation of ICs and Systems* pp 1–4
[16] Zhang Y, Edwards M, Samani M K, Logothetis N, Ye L, Fu Y, Jeppson K and Liu J 2016 Characterization and simulation of liquid phase exfoliated graphene-based films for heat spreading applications *Carbon* **106** 195–201
[17] Lee X *et al* 2013 Flexible graphene woven fabrics for touch sensing *Appl. Phys. Lett.* **102** 163117
[18] Wu J, Agrawal M, Becerril H A, Bao Z, Liu Z, Chen Y and Peumans P 2010 Organic light-emitting diodes on solution-processed graphene transparent electrodes *ACS Nano* **4** 43–48
[19] Bae S, Kim S J, Shin D, Ahn J-H and Hong B H 2012 Towards industrial applications of graphene electrodes *Phys. Scr.* **2012** 014024
[20] Yin Z, Zhu J, He Q, Cao X, Tan C, Chen H, Yan Q and Zhang H 2014 Graphene-based materials for solar cell applications *Adv. Energy Mater.* **4** 1300574
[21] Jang H, Park Y J, Chen X, Das T, Kim M-S and Ahn J-H 2016 Graphene-based flexible and stretchable electronics *Adv. Mater.* **28** 4184–202
[22] Georgakilas V, Tiwari J N, Kemp K C, Perman J A, Bourlinos A B, Kim K S and Zboril R 2016 Noncovalent functionalization of graphene and graphene oxide for energy materials, biosensing, catalytic, and biomedical applications *Chem. Rev.* **116** 5464–519
[23] Maine E P S 2016 Graphene steps into biomedicine *Nat. Mater.* **15** 485
[24] Tzalenchuk A, Lara-Avila S, Kalaboukhov A, Paolillo S, Syväjärvi M, Yakimova R, Kazakova O, Janssen T J B M, Fal'ko V and Kubatkin S 2010 Towards a quantum resistance standard based on epitaxial graphene *Nat. Nanotech.* **5** 186–9
[25] Berger C *et al* 2004 Ultrathin epitaxial graphite: 2D electron gas properties and a route toward graphene-based nanoelectronics *J. Phys. Chem.* B **108** 19912–6
[26] Hass J, Heer de W A and Conrad E H 2008 The growth and morphology of epitaxial multilayer graphene *J. Phys. Condens. Matter* **20** 323202
[27] Kim K S, Zhao Y, Jang H, Lee S Y, Kim J M, Kim K S, Ahn J-H, Kim P, Choi J-Y and Hong B H 2009 Large-scale pattern growth of graphene films for stretchable transparent electrodes *Nature* **457** 706–10
[28] Li X *et al* 2009 Large-area synthesis of high-quality and uniform graphene films on copper foils *Science* **324** 1312–4
[29] Stankovich S, Piner R D, Nguyen S T and Ruoff R S 2006 Synthesis and exfoliation of isocyanate-treated graphene oxide nanoplatelets *Carbon* **44** 3342–7
[30] Liu -W-W, Chai S-P, Mohamed A R and Hashim U 2014 Synthesis and characterization of graphene and carbon nanotubes: a review on the past and recent developments *J. Ind. Eng. Chem.* **20** 1171–85
[31] Son M and Ham M-H 2017 Low-temperature synthesis of graphene by chemical vapor deposition and its applications *FlatChem* **5** 40–49
[32] Seah C-M, Chai S-P and Mohamed A R 2014 Mechanisms of graphene growth by chemical vapour deposition on transition metals *Carbon* **70** 1–21
[33] Mu W, Fu Y, Sun S, Edwards M, Ye L, Jeppson K and Liu J 2016 Controllable and fast synthesis of bilayer graphene by chemical vapor deposition on copper foil using a cold *Wall Reactor Chem. Eng. J.* **304** 106–14
[34] Park H J, Meyer J, Roth S and Skákalová V 2010 Growth and properties of few-layer graphene prepared by chemical vapor deposition *Carbon* **48** 1088–94
[35] Gao L *et al* 2012 Repeated growth and bubbling transfer of graphene with millimetre-size single-crystal grains using platinum *Nat. Commun.* **3** 699
[36] McLellan R B 1969 The solubility of carbon in solid gold, copper, and silver *Scr. Metall.* **3** 389–91
[37] Longson B and Thorley A W 1970 Solubility of carbon in sodium *J. Chem. Technol. Biotechnol.* **20** 372–9
[38] Wu T *et al* 2016 Fast growth of inch-sized single-crystalline graphene from a controlled single nucleus on Cu–Ni alloys *Nat. Mater.* **15** 43–47
[39] Zhang Y, Fu Y, Edwards M, Jeppson K, Ye L and Liu J 2017 Chemical vapor deposition grown graphene on Cu-Pt alloys *Mater. Lett.* **193** 255–8
[40] Li X, Colombo L and Ruoff R S 2016 Synthesis of graphene films on copper foils by chemical vapor deposition *Adv. Mater.* **28** 6247–52
[41] Lander J J, Kern H E and Beach A L 1952 Solubility and diffusion coefficient of carbon in nickel: reaction rates of nickel-carbon alloys with barium oxide *J. Phys. D: Appl. Phys.* **23** 1305–9
[42] Liu L *et al* 2016 A mechanism for highly efficient electrochemical bubbling delamination of CVD-Grown graphene from metal substrates *Adv. Mater. Interfaces* **3** 1500492
[43] Roddaro S, Pingue P, Piazza V, Pellegrini V and Beltram F 2007 The optical visibility of graphene: interference colors of ultrathin graphite on SiO2 *Nano Lett.* **7** 2707–10
[44] Blake P, Hill E W, Castro Neto A H, Novoselov K S, Jiang D, Yang R, Booth T J and Geim A K 2007 Making graphene visible *Appl. Phys. Lett.* **91** 063124
[45] Regan W, Alem N, Alemán B, Geng B, Girit Ç, Maserati L, Wang F, Crommie M and Zettl A 2010 A direct transfer of layer-area graphene *Appl. Phys. Lett.* **96** 113102
[46] de la Rosa C J L, Sun J, Lindvall N, Cole M T, Nam Y, Löffler M, Olsson E, Teo K B K and Yurgens A 2013 Frame assisted H2O electrolysis induced H2 bubbling transfer of

large area graphene grown by chemical vapor deposition on Cu *Appl. Phys.Lett.* **102** 022101
[47] Eckmann A, Felten A, Verzhbitskiy I, Davey R and Casiraghi C 2013 Raman study on defective graphene: effect of the excitation energy, type, and amount of defects *Phys. Rev.* B **88** 035426
[48] Wu J-B, Lin M-L, Cong X, Liu H-N and Tan P-H 2018 Raman spectroscopy of graphene-based materials and its applications in related devices *Chem. Soc. Rev.* **47** 1822–73
[49] Stroscio J A, Bare S R and Ho W 1984 The chemisorption and decomposition of ethylene and acetylene on Ni(110) *Surf. Sci.* **148** 499–525
[50] Marinova T S and Stefanov P K 1987 Adsorption and thermal evolution of acetylene on a Cu(100) surface *Surf. Sci.* **191** 66–74
[51] Lehwald S and Ibach H 1979 Decomposition of hydrocarbons on flat and stepped Ni(111) surfaces *Surf. Sci.* **89** 425–45
[52] López G A and Mittemeijer E J 2004 The solubility of C in solid Cu *Scr. Mater.* **51** 1–5
[53] Li X, Cai W, Colombo L and Ruoff R S 2009 Evolution of graphene growth on Ni and Cu by carbon isotope labeling *Nano Lett.* **9** 4268–72